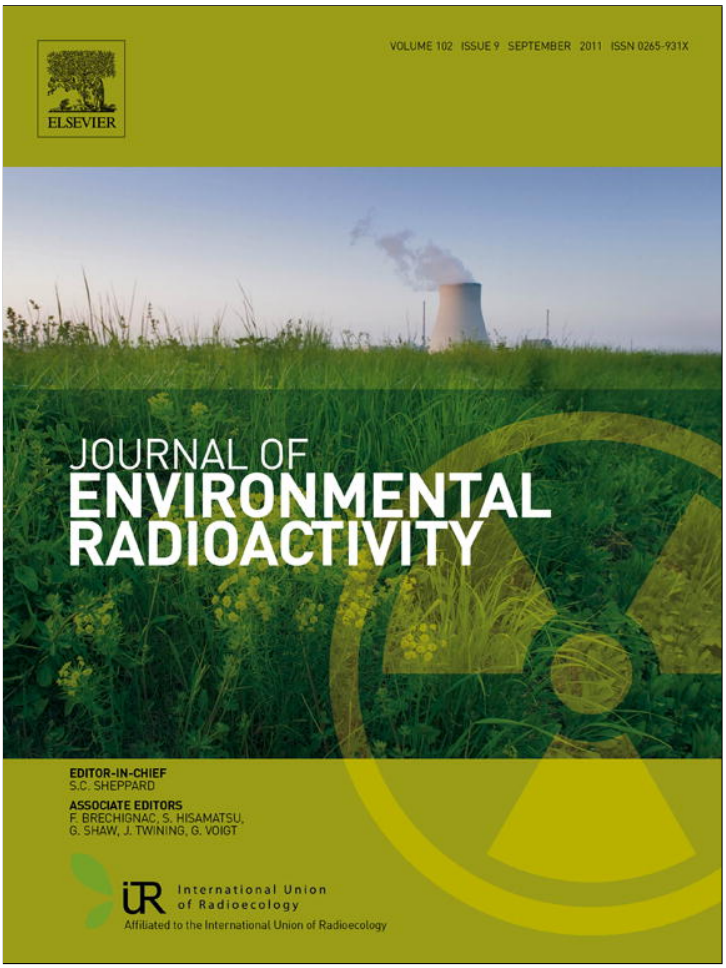

Journal of Environmental Radioactivity 102 (2011) 863–870

Contents lists available at ScienceDirect

Journal of Environmental Radioactivity

journal homepage: www.elsevier.com/locate/jenvrad

Spatial distribution of soil radon as a tool to recognize active faulting on an active volcano: the example of Mt. Etna (Italy)

Marco Neri [a,*], Salvatore Giammanco [a], Elisabetta Ferrera [b], Giuseppe Patanè [b], Vittorio Zanon [c]

[a] Istituto Nazionale di Geofisica e Vulcanologia, Piazza Roma, 2 – 95123 Catania, Italy
[b] Università degli Studi di Catania, Dip. Scienze della Terra, Corso Italia, 52 – 95129 Catania, Italy
[c] Centro de Vulcanologia e Avaliação de Riscos Geológicos – Universidade dos Açores, Rua Mãe de Deus, 9501-801 Ponta Delgada, Portugal

ARTICLE INFO

Article history:
Received 7 January 2011
Received in revised form
12 April 2011
Accepted 5 May 2011
Available online 25 June 2011

Keywords:
Radon
Fault
Seismic hazard
Etna

ABSTRACT

This study concerns measurements of radon and thoron emissions from soil carried out in 2004 on the eastern flank of Mt. Etna, in a zone characterized by the presence of numerous seismogenic and aseismic faults. The statistical treatment of the geochemical data allowed recognizing anomaly thresholds for both parameters and producing distribution maps that highlighted a significant spatial correlation between soil gas anomalies and tectonic lineaments. The seismic activity occurring in and around the study area during 2004 was analyzed, producing maps of hypocentral depth and released seismic energy. Both radon and thoron anomalies were located in areas affected by relatively deep (5–10 km depth) seismic activity, while less evident correlation was found between soil gas anomalies and the released seismic energy. This study confirms that mapping the distribution of radon and thoron in soil gas can reveal hidden faults buried by recent soil cover or faults that are not clearly visible at the surface. The correlation between soil gas data and earthquakes depth and intensity can give some hints on the source of gas and/or on fault dynamics.

1. Introduction

Radon is a radioactive, noble gas which is present in all the rocks of the Earth. It is currently used by the scientific community as a tracer of natural phenomena linked to soil degassing along faults, fractures and crustal discontinuities (Israel and Bjornsson, 1967; King et al., 1996; Mazur et al., 1999; Jonsson et al., 1999; Choubey et al., 1999; Durrani, 1999; Baubron et al., 2002; Vaupotič, 2003). Recently, radon was also used on Mt. Etna both as a precursor of volcanic phenomena (Alparone et al., 2005; Morelli et al., 2006; Neri et al., 2006; Giammanco et al., 2007) and in the study of the dynamics of active faults (Immè et al., 2006a,b; Neri et al., 2007; La Delfa et al., 2007a; Giammanco et al., 2009; Siniscalchi et al., 2010), including those that are hidden by recent lavas or tephra cover (Burton et al., 2004). This paper shows ~200 measurements of radon sampled in a key area of Etna from a tectonic point of view, covering an area of ~20 km^2. Our study is the first one that covers such a wide area by performing such a high number of radon and thoron measurements in soil. Therefore, the results are interesting not only for their implications on tectonics and earthquake mechanisms, but also for a better understanding of how radon distributes over large surfaces and how it behaves in terms of transport dynamics in soil with different permeability.

Radon has a mass of 86 and it has thirty-seven known isotopes according to ENSDF (2011), or forty-three according to Sonzogni (2008) and Nuclear Wallet Cards (2009). The three most common radon isotopes in nature are ^{222}Rn (radon), ^{220}Rn (thoron) and ^{219}Rn (actinon). The ^{222}Rn is produced by α decay from ^{226}Ra, it has a mean half-life of 3.8 days and belongs to the decay family of ^{238}U. Thoron is produced by α decay of ^{224}Ra, it has a mean half-life of 55 s and belongs to the radioactive decay chain of ^{232}Th. Actinon has a mean half-life of only 4 s and derives from ^{235}U.

Of the three main isotopes, ^{222}Rn is the most useful for geochemical surveys because its half-life is long enough to allow its diffusive transport through relatively thick layers of soil or other materials. For this reason, under conditions of scarce dilution (poor aeration), such as those encountered in some closed indoor environments, its concentration in the atmosphere can be high (ICRP-65, 1993; Žunić et al., 2006; Brogna et al., 2007; Malczewski and Żaba, 2007).

As the half-life of ^{220}Rn is relatively short, it is proven to be useful only in areas where advective transport of soil gas is particularly high and/or in areas where there are rocks containing significant amounts of Th-rich mineral phases, such as biotite,

* Corresponding author. Tel.: +39 0957165858; fax: +39 095 7165826.
E-mail address: marco.neri@ct.ingv.it (M. Neri).

0265-931X/$ – see front matter © 2011 Elsevier Ltd. All rights reserved.
doi:10.1016/j.jenvrad.2011.05.002

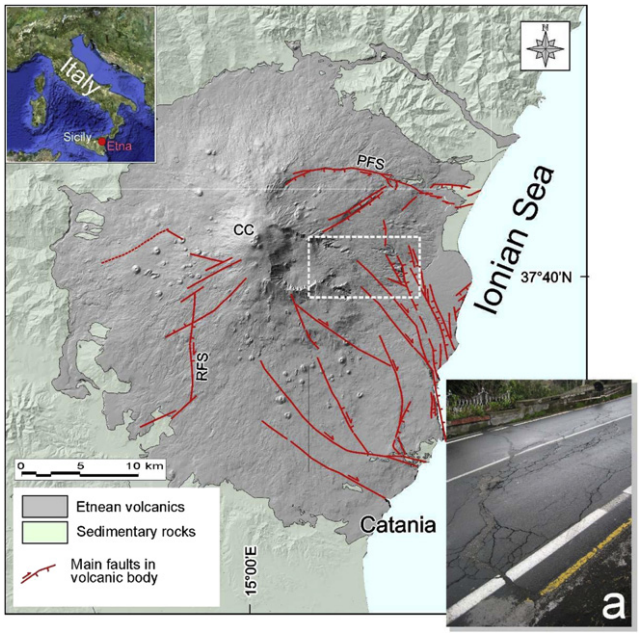

Fig. 1. Simplified structural map of Mt. Etna (after Neri et al., 2009) and location of the study area (white dashed box). Inset (a): seismogenetic surface faulting (NW–SE) affecting a road on the eastern flank of Mount Etna, occurring during the first stage of the 2002–2003 eruption. The northwestern portion of this fault is located in the studied area. CC = Central craters; PFS = Pernicana fault system; RFS = Ragalna fault system.

apatite and sphene. However, the highest concentrations of this element occur in accessory phases such as allanite, thorite, uraniumthorite, thorianite, monazite and zircon (Casillas et al., 1995; Wang et al., 2001).

Lastly, the role of ^{219}Rn in geochemical exploration is negligible, due to its very short half-life that causes its decay in the soil before it can reach the atmosphere. Only emissions of radon and thoron gases from the soil, therefore, can give information on the increase of magmatic and seismic activity, mostly in the areas with high crustal permeability (Giammanco et al., 2007, and references therein).

Mt. Etna (Sicily, Southern Italy) is the largest active volcano in continental Europe, with a diameter of more than 35 km and a height of about 3329 m (Neri et al., 2008). Its frequent eruptions occur both from the four summit craters and from the three fissure zones (or "rift") which are present on its flanks to converge uphill towards the summit (Acocella and Neri, 2003, and references therein). The area surrounding the volcano has been populated since pre-Roman times. Diffuse urbanization of this area and anthropic activities (i.e. vineyards, fruit orchards) have substantially changed the existing landforms and often obliterated the shallow geomorphology features since the Middle Ages. Moreover, commonly with other active volcanoes, constructive/destructive processes typically operate frequent and deep morphological changes, especially in the summit area (Behncke et al., 2004; Neri et al., 2008).

Several earthquakes occur every day in the area of Mt. Etna, more numerous in the eastern flank (http://www.ct.ingv.it/ufs/analisti/). Despite their typical low to very low magnitude ($M < 2$), they deserve to be studied for a complete understanding of the volcano dynamics (Acocella et al., 2003; Burton et al., 2005, and references therein). As we will demonstrate in this paper, a correlation between seismicity and soil radon measurements carried out in 2004 was found, which permitted to discover several active hidden faults located in the mid-lower eastern flank of the volcano, and allowed us to set up a method potentially useful to forecast seismic activity.

2. The study area

The present study was carried out in the mid-lower east flank of Mt. Etna, in an area between the villages of Milo and Zafferana Etnea (white dashed box in Fig. 1). Measurements of radon and thoron emissions from soil were performed in this area because of the presence of numerous active faults, both seismogenic and aseismic (Burton et al., 2004; Walter et al., 2005; Neri et al., 2005; Monaco et al., 2008), which generated frequent historical quakes with maximum magnitude of 4.5 (15 October 1911, Imposa and Patané, 1985). Furthermore, the area is subject to slow but constant gravitational sliding towards the SE (Solaro et al., 2010 and references therein). This mobile sector is bounded to the north by the E-W-running Pernicana Fault System (PFS in Fig. 1), with average motion rate ranging between a few millimeters and 2–3 cm a^{-1} (Acocella and Neri, 2005) and to the southwest by the Ragalna Fault System (RSF; Neri et al., 2007; Fig. 1), affecting an onshore area of >700 km^2 (Neri et al., 2004). The unstable sector is also divided into at least seven minor blocks characterized by different kinematics and bounded by faults (Solaro et al., 2010). The last violent seismic sequence affecting the study area occurred in 2002, during the first stages of the 2002–2003 flank eruption that triggered a vast gravitational sliding of a large portion of Etna's east flank (Neri et al., 2004).

3. Sampling and analytical methods

Between January 21st and October 7th of 2004, 227 measurements of radon and thoron from soil were carried out. Measurements were performed following a sampling grid of points that was kept as regular as possible, although the final geometry was affected by logistics (inaccessible areas, private properties, etc.). Because measurements were carried out in different periods (and seasons) of the year, they could be affected by variable environmental conditions and/or by variable degassing levels of the volcano/tectonic system. This could make the data not intercomparable. However, recent works carried out on soil CO_2 emissions from several areas of Mt. Etna (Giammanco and Bonfanti, 2009; Giammanco et al., 2010) showed that repeated samplings of soil gases over large areas during long periods of time did not

Table 1
Basic statistics for the soil radon and soil thoron activity data (both raw and Log_{10}-transformed) from the study area.

	N total	Mean	Stand. dev.	Skewness	Minimum	Median	Maximum
Results for the raw data							
Radon	227	10,100	11,000	1.82	267	6230	52,000
Thoron	227	14,600	12,000	1.24	31.3	12,900	64,600
Results for the log_{10}-transformed data							
Radon	227	3.75	0.51	−0.26	2.42	3.79	4.72
Thoron	227	3.95	0.54	−1.49	1.49	4.11	4.81

alter the location of anomalous soil gas emissions, although anomalous sites showed marked changes of their absolute degassing values in time. Therefore, assuming that the general behavior of ^{222}Rn and ^{220}Rn is similar to that of CO_2, which applies at least for relatively low fluxes of the carrier gas for radon (Giammanco et al., 2007), the sampling strategy used in this work can be considered reasonably valid and the anomalous sites can be assumed as stable, thus making the spatial analysis of data reliable.

Measurements were carried out using a portable electronic detector (mod. RAD7, Durridge Company Inc., USA). This detector measures concentrations of both ^{222}Rn (radon) and ^{220}Rn (thoron) in the bulk sampled gas phase, by counting the alpha particles emitted by the decay of their respective daughter nuclides ^{218}Po ($t^{1/2} = 3.04$ min) and ^{216}Po ($t^{1/2} = 0.145$ s). The soil gas is extracted from the ground at 40 cm depth by an internal pump and the measurements require approximately 15 min, in order to reach equilibrium with the measured daughter nuclide ^{218}Po.

We tested if the distribution of data in our survey was normal or not by using some basic statistical tools (Davis, 1986), calculating the mean, median and skewness of sample populations. This is a necessary step because soil radon and thoron values, following one of the fundamental laws of geochemistry (Ahrens, 1954), are usually log-normally distributed and hence raw data need to be transformed into their log values.

Furthermore, in order to assess the anomaly threshold for soil radon and thoron activities, logarithmic probability plots were used for the data gathered in the area, assuming a log-normal distribution of values. Sinclair (1974) discussed that in such plots, changes in the slope of cumulated values are indicative of separate populations of data. Finally, we used kriging interpolation method to produce two-dimensional distribution maps of radon and thoron values in the area. Seismicity data are collected from the data-base of the Istituto Nazionale di Geofisica e Vulcanologia - Catania Department (INGV-Ct), available at http://www.ct.ingv.it/.

4. Results and discussion

4.1. Radon and thoron surveys

The results obtained from the 2004 survey are summarized in Table 1. Radon values ranged from 266 to 52,000 Bq m^{-3} (arithmetic mean $\bar{x} = 10,133$ Bq m^{-3}; standard deviation 1σ = 10,969 Bq m^{-3}). Thoron values ranged from 31 to 64,550 Bq m^{-3} ($\bar{x} = 14,575$ Bq m^{-3}; $1\sigma = 11,963$ Bq m^{-3}). Histograms of frequency distribution of raw values of radon (a) and thoron (b) are shown in Fig. 2. The distribution of values of both parameters shows a divergence between mean and median values of each data-set and high positive values of the skewness obtained from their frequency distributions (Table 1). This is indicative of a log-normal distribution of the data. Therefore, we calculated the Log_{10} of all activity values measured and we operated all further statistics on these transformed data, which resulted in clear Gaussian distributions (Fig. 3), as also indicated by the small divergence between mean and median values of each data-set and the negative skewness values obtained from the Log_{10} frequency distributions (Table 1).

The logarithmic probability plot of the Log_{10} values of ^{222}Rn data (Fig. 4a) indicates three inflection points, respectively at the percentiles 71, 91 and 96, suggesting the presence of four distinct populations. The average soil ^{222}Rn values of the four populations are 3200 Bq m^{-3}, 17,000 Bq m^{-3}, 32,000 Bq m^{-3} and 46,000 Bq m^{-3}, respectively. The logarithmic probability plot of the Log_{10} values of ^{220}Rn data (Fig. 4c) indicates three inflection points as well, respectively at the percentiles 71, 91 and 96, suggesting again the presence of four distinct populations. The average soil

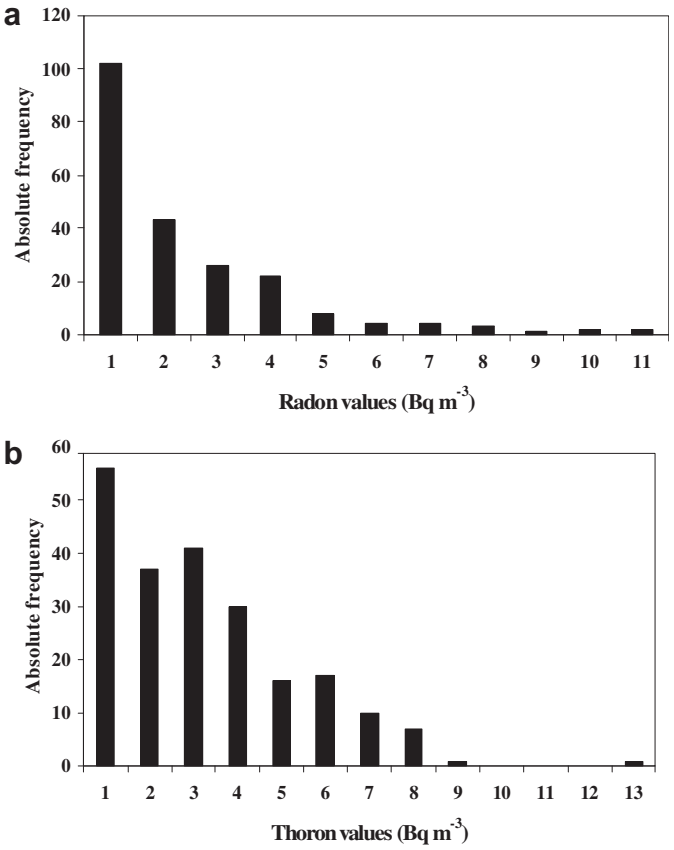

Fig. 2. Histograms of frequency distribution of raw values of radon (a) and thoron (b).

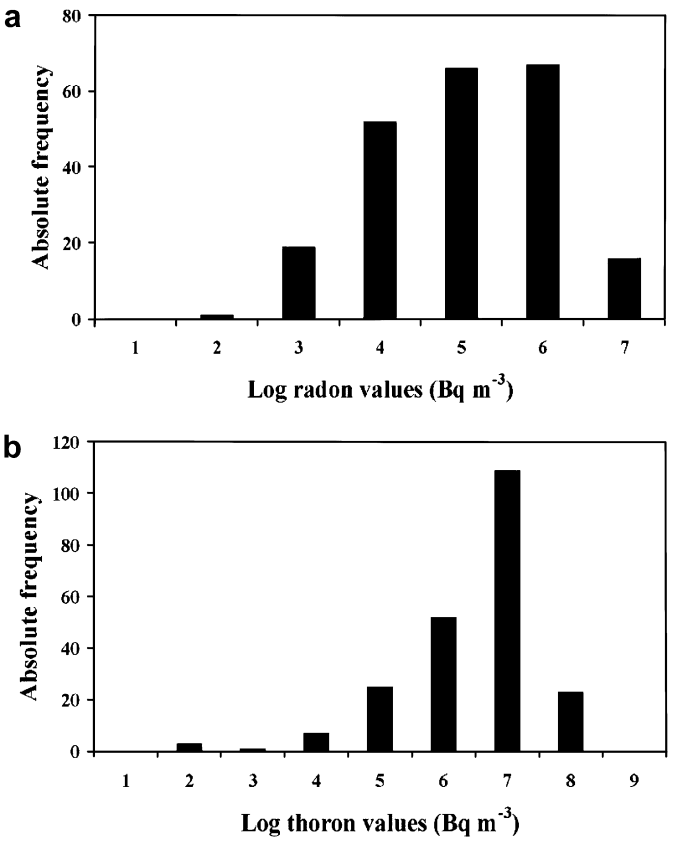

Fig. 3. Histograms of frequency distribution of Log values of radon (a) and thoron (b).

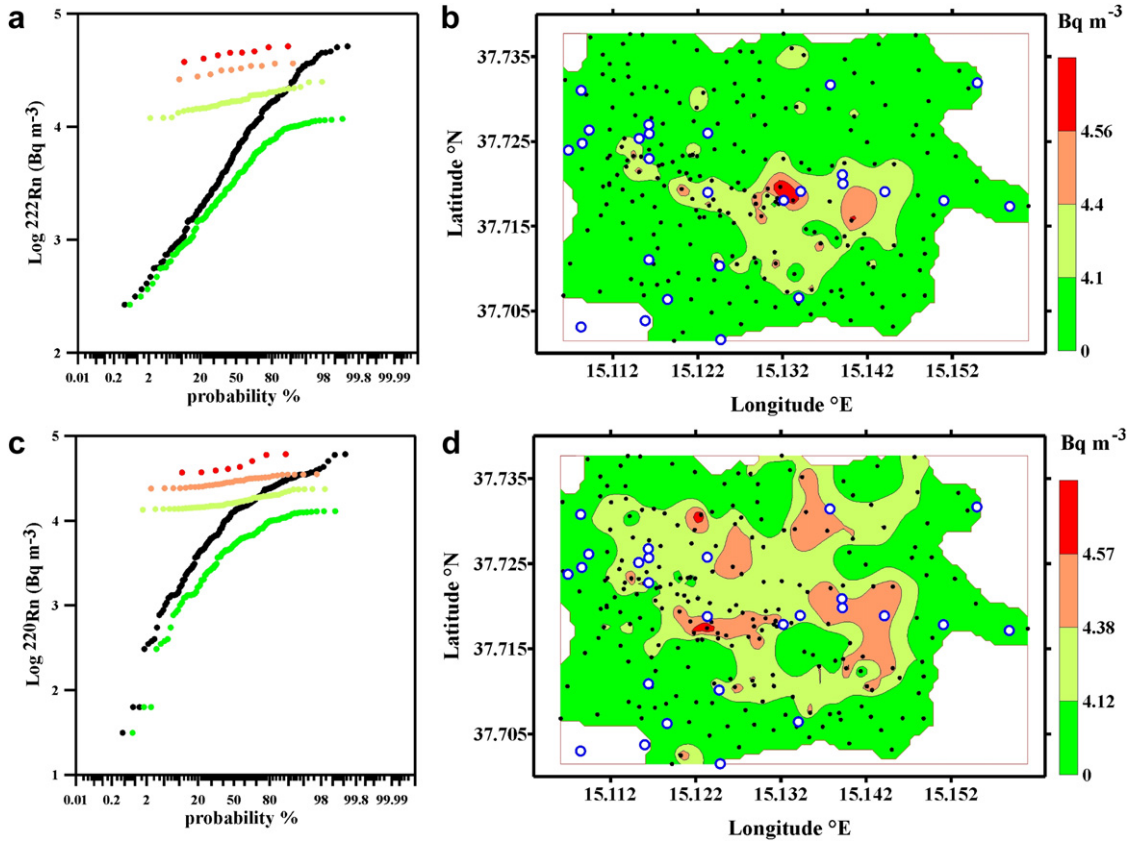

Fig. 4. Normal probability plots of the Log values of radon (a) and thoron (c) using the method of Sinclair (1974). Distribution maps of the Log values of radon (b) and thoron (d) in the study area (interpolation method = kriging). In these maps, classes of values were chosen based on the inflection points obtained in the normal probability plots. For each single population of both parameters, we recalculated the cumulative values applying the same procedure as that used for the entire data-set. The results show almost linear distributions of recalculated data in most of the cases, thus confirming that such populations are statistically distinct and homogeneous within themselves. White dots in figures (b) and (d) represent the spatial distribution of epicentral location of earthquakes that occurred in the studied area during 2004.

^{220}Rn values of the four populations are 3800 Bq m^{-3}, 17,000 Bq m^{-3}, 29,000 Bq m^{-3} and 47,000 Bq m^{-3}, respectively. The basic statistics for each population in both plots are shown in Table 2.

In both plots, the populations with the lowest cumulative values (populations A) represent the background levels for radon and thoron, respectively. The other populations represent possible anomalous values, with increasing intensity. Following the procedure described by Sinclair (1974), we recalculated cumulative values for the single "anomalous" populations of each parameter applying the same procedure as that used for the entire data-set. The results show almost linear distributions in both cases (Fig. 4a and c), thus confirming that such populations are statistically distinct and homogeneous within themselves.

Table 2
Estimated parameters of partitioned populations of soil radon and thoron activities. f_i indicates the proportion of total observations in each subpopulation. Subscript i refers to the ith partitioned population.

	Population	N	f_i (%)	Mean (Log Bq m^{-3})	Min–Max (Log Bq m^{-3})
^{222}Rn	A	161	70.9	3.50	2.42–4.07
	B	46	20.3	4.24	4.08–4.40
	C	11	4.8	4.51	4.41–4.56
	D	9	4.0	4.66	4.57–4.72
	Σ	227	100		
^{220}Rn	A	117	51.5	3.58	1.49–4.13
	B	62	27.3	4.23	4.13–4.38
	C	39	17.2	4.46	4.38–4.56
	D	9	4.0	4.67	4.57–4.81
	Σ	227	100		

Based on the four populations obtained with the normal probability plots, maps were produced that show the spatial distribution of activity values both of radon and of thoron in the studied area (Fig. 4b and d). Both distribution maps show a clear zone with greater intensity of soil radon and thoron emission, located in the central part of the study area and directed roughly NW–SE. The anomaly is better defined in the case of radon values, whereas thoron values show other anomalous zones in the northern part of the study area.

4.2. Radon and seismic activity in 2004

Twenty-six out of 539 Etnean seismic events detected by the seismic network of INGV-Ct, during 2004, occurred inside the studied area with focal depths <20 km. In particular, some of these earthquakes were located near sites where radon values were markedly high and were aligned following an apparent NW–SE direction (Fig. 4), thus in agreement with the direction of the inferred faults described.

However, to analyze local seismic activity in a way that is more representative of the dynamics of the sector of Etna where the study area was located, it was necessary to consider a wider area of incidence of seismicity (Fig. 5). In this larger area, ninety earthquakes occurring between January 6th and December 28th, 2004 and with hypocenters <20 km were selected. The hypocentral distribution of those earthquakes is shown in the map of Fig. 5.

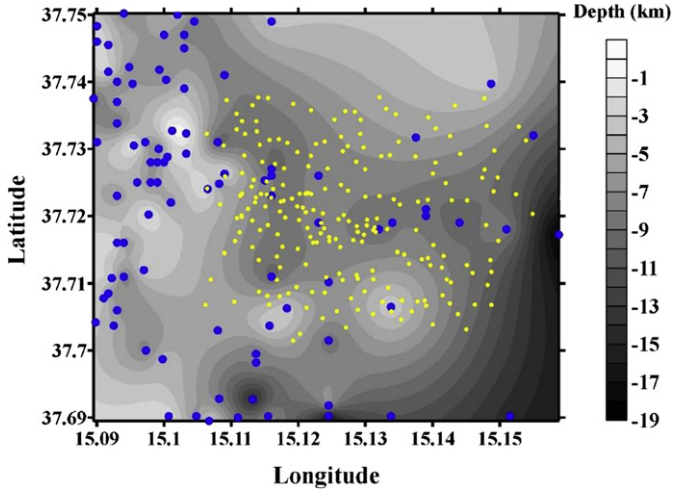

Fig. 5. Distribution map of hypocentral depth of earthquakes in the study area (interpolation method = kriging). Blue dots show the location of earthquake epicenters. Yellow dots show the location of soil gas sampling points. The map shows that in general seismic activity becomes deeper (>10 km) on moving towards the SE corner and the central part of the study area. (For interpretation of the references to color in this figure legend, the reader is referred to the web version of this article.)

The map was built considering classes of hypocentral depths with a difference of 1 km. The map shows that, in general, shallow earthquakes (<10 km) prevail in the western part of the area and, to a lesser extent, also in its northern part. Conversely, deeper earthquakes are located near the SE corner of the area. Nevertheless, deep seismic events are also located in a relatively narrow zone of the central part of the area.

By plotting the cumulate frequency distribution of seismic energy (in Log values) for those earthquakes (Fig. 6) it is possible to distinguish different subpopulations. The basic statistics for each subpopulation are shown in Table 3. The seismic energy distribution map for the events of the area exposed in Fig. 5 is also shown in Fig. 7. In general, the energy released by earthquakes during 2004 was of average intensity compared with the typical values of Mt. Etna area (see the INGV-CT data-base available at http://www.ct.ingv.it/). In the larger area considered (See Fig. 5), earthquakes occurring in its southern and northwestern sectors were characterized by the highest energy release, with a general faint WNW-ESE orientation (Fig. 7). Furthermore, as the depth of earthquakes increases, there seems to be a slight tendency towards a higher seismic energy release (the Pearson correlation coefficient between the two variables is only 0.15).

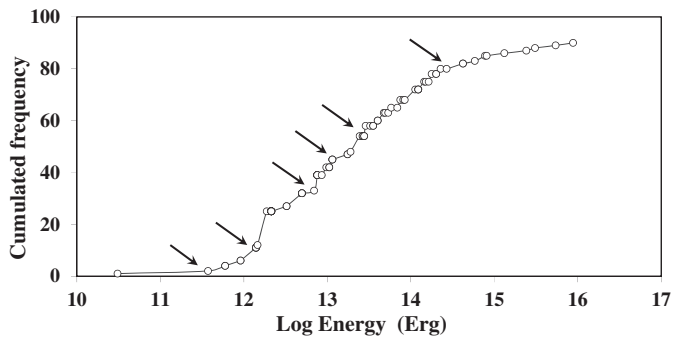

Fig. 6. Cumulate frequency distribution of the Log values of seismic energy released in the study area during 2004. Classes of values were chosen based on the inflection points and were used to construct the map in Fig. 7. Arrows indicate inflection points.

Table 3
Estimated parameters of partitioned populations of seismic energy. f_i indicates the proportion of total observations in each subpopulation. Subscript i refers to the ith partitioned population.

Population	*N*	f_i (%)	Mean (Log erg)	Min–Max (Log erg)
A	1	1.1	10.5	10.5–10.5
B	11	12.2	12.0	11.6–12.2
C	20	22.2	12.4	12.3–12.7
D	15	16.7	13.0	12.8–13.2
E	8	8.9	13.4	13.3–13.4
F	24	26.7	13.9	13.5–14.3
G	11	12.2	15.1	14.4–15.9
Total	90	100.0		

The maps of hypocentral distribution and seismic energy release described above were compared with the distributions of soil radon and thoron and with the location of local tectonic faults (Fig. 8). Fig. 8a highlights the spatial correspondence between radon anomalies and the occurrence of earthquakes with hypocenters at medium depth (5–10 km) in the central sector of the study area. This sector is also cut by NW–SE and WNW–ESE faults with strike–slip movement components. One of these faults is marked by a distinctly visible scarp in the field, but two other fault segments were hidden and could only be discontinuously observed at the surface during co-seismic ground fracturing, as in the case of the October–November 2002 seismic crisis (Burton et al., 2004; Neri et al., 2005).

Fig. 8a also shows that the shallowest hypocenters (<5 km) occurred mostly in the western sector of the study area, where radon and thoron emissions were relatively low. This sector is also cut by another fault segment characterized by co-seismic ground fracturing that highlighted a prevailing right-lateral component of movement (Acocella et al., 2003; Burton et al., 2004; Walter et al., 2005; Neri et al., 2005).

Soil radon and thoron anomalies seem to occur in sectors of the study area characterized by low seismic energy release (Fig. 8b), so the key factor in determining voluminous radon and thoron soil release seems to be represented by the depth of earthquake hypocenters rather than the intensity of seismic activity. However, even this consideration provides useful information on the

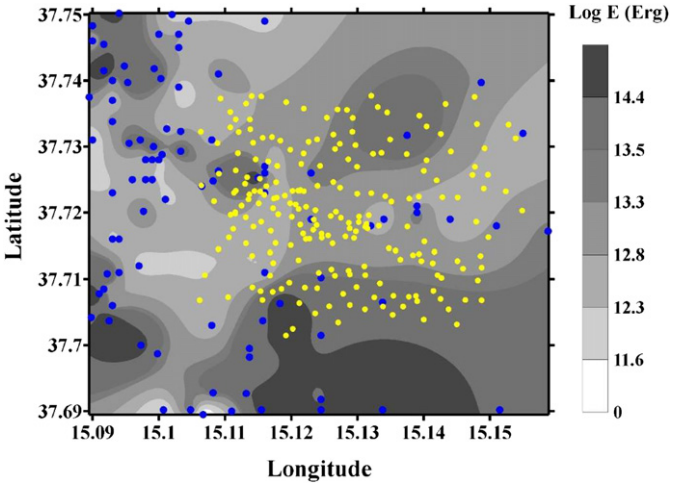

Fig. 7. Distribution map of seismic energy released in the study area during 2004 (interpolation method = kriging). Blue dots show the location of earthquakes epicenters. Yellow dots show the location of soil gas sampling points. (For interpretation of the references to color in this figure legend, the reader is referred to the web version of this article.)

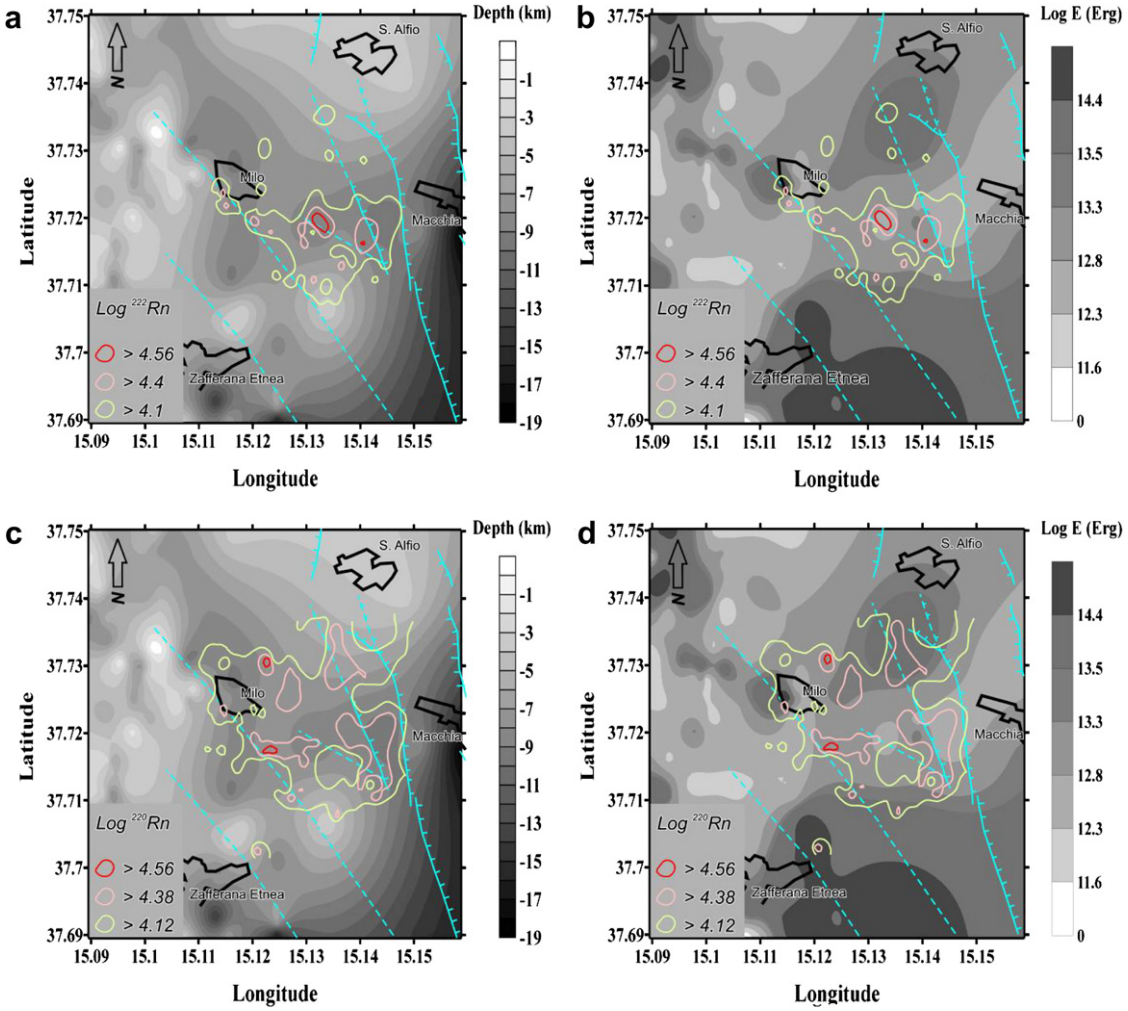

Fig. 8. Structural maps of the investigated area overlapped to the map of distribution of radon anomalies (activity values >4.1 in Log units, as obtained from Fig. 4) and to a) the distribution map of hypocentral depth of local earthquakes (as obtained from Fig. 5) and b) the distribution map of seismic energy release (as obtained from Fig. 7). Solid blue lines indicate faults with surface evidence (bars on downthrown side); dashed blue lines indicate fault segments that are hidden or with prevailing strike–slip movements (from Neri et al., 2009).

rheology of the crust in the area concerned. In our opinion, it is no accident that the major radon emission coincides with the location where earthquakes have relatively deep hypocenters and show lower magnitude than those of the surrounding areas. This phenomenon could be due to the rising of rather hot fluids favoring the migration of radon to the surface influencing brittle and ductile deformation processes, the latter not detectable by traditional seismic stations (La Delfa et al., 2007b).

According to the above data, radon seems to be released mostly through relatively deep (5–10 km) tectonic structures that run along NW–SE directions. The highest radon anomalies were located where these faults intersect shallower (<5 km) WNW–ESE tectonic structures characterized by prevalent strike–slip mechanism. Nevertheless, the identification of the presence/position of active hidden faults, at greater detail, needs radon surveys with a higher spatial resolution (sampling points spaced a few meters to some tens of meters apart; Burton et al., 2004). This extension in the investigation could represent the next step and one of the most attractive eventual results for this study, in order to increase our ability to assess the local risk posed by volcano-tectonic earthquakes and aseismic movement along creeping faults.

5. Conclusions

The present work provided useful information on the geochemical behavior both of radon and thoron from soil gas emissions in an active seismic area of Mt. Etna Volcano. The evaluation of the statistical treatment of the geochemical data-base allowed us to recognize anomaly thresholds for both parameters and to produce maps of distribution that highlighted a significant spatial correlation between soil gas anomalies and tectonic lineaments in the central part of study area. In particular, the highest anomalies were found at the intersection between WNW–ESE and NW–SE-running faults.

The statistical analysis of the seismic activity that occurred in and around the study area during 2004 led to the production of distribution maps both of the depth of hypocenters and of the released seismic energy. These maps revealed a progressive deepening of hypocenters from NW to SE, with the exception of a narrow zone in the central part of the area, with a roughly WNW–ESE direction. Also, the highest values of seismic energy were released during events in the southern and northwestern sectors of the area.

By overlapping the maps of radon and thoron anomalies to those of earthquake hypocentral depths and seismic energy, we observed that both radon and thoron anomalies were located on areas affected by relatively deep (5–10 km depth) seismic activity. A less evident correlation was found between soil gas anomalies and the released seismic energy. This study shows that mapping the distribution of radon and thoron in soil gas is an effective way to reveal hidden faults buried by recent soil cover or faults that are not clearly visible at the surface. The correlation between soil gas data and earthquakes depth and intensity can give some hints on the source of gas and/or on fault dynamics.

Lastly, an important spin-off of this study is the recognition of some areas where radon activity was so high ($>$50,000 Bq m^{-1}, see Table 1) that it may represent a potential hazard to the local population. In fact, radon is the leading cause of lung cancer after cigarette smoke for long exposures (WHO-IARC, 1988) and, due to its molecular weight, it accumulates in underground rooms or in low ground, particularly where air circulation is low or absent. In the investigated area this risk is real, as it is inhabited by thousands of people who reside there all year long. Therefore, this study serves as a starting point for the assessment of radon hazard in the Mt. Etna area, considering both spatial and temporal changes in soil radon emissions depending on the presence of faults and/or the occurrence of seismic activity.

Acknowledgments

This work was made possible thanks to a collaboration between the Istituto Nazionale di Geofisica e Vulcanologia – Sezione di Catania and the Università di Catania, Dipartimento di Scienze della Terra. Domenico Condarelli provided a valid contribution during the field work to acquire part of the data on radon and thoron. The authors thank two anonymous reviewers and the editor S. C. Sheppard for their helpful and constructive comments. Steve Conway provided language help.

References

Acocella, V., Behncke, B., Neri, M., D'Amico, S., 2003. Link between major flank slip and eruptions at Mt. Etna (Italy). Geophys. Res. Lett. 30 (24), 2286. doi:10.1029/2003GL018642.

Acocella, V., Neri, M., 2003. What makes flank eruptions?: the 2001 Etna eruption and the possible triggering mechanisms. Bull. Volcanol. 65, 517–529. doi:10.1007/s00445-003-0280-3.

Acocella, V., Neri, M., 2005. Structural features of an active strike–slip fault on the sliding flank of Mt. Etna (Italy). J. Struct. Geol. 27 (2), 343–355. doi:10.1016/j.jsg.2004.07.006.

Alparone, S., Behncke, B., Giammanco, S., Neri, M., Privitera, E., 2005. Paroxysmal summit activity at Mt. Etna monitored through continuous soil radon measurements. Geophys. Res. Lett. 32, L16307. doi:10.1029/2005GL023352.

Ahrens, L.H., 1954. The lognormal distribution of the elements (A fundamental law of geochemistry and its subsidiary). Geochim. Cosmochim. Acta 5, 49–73.

Behncke, B., Neri, M., Sturiale, G., 2004. Rapid morphological changes at the summit of an active volcano: reappraisal of the poorly documented 1964 eruption of Mount Etna (Italy). Geomorphology 63 (3–4), 203–218. doi:10.1016/j.geomorph.2004.04.004.

Baubron, J.-C., Rigo, A., Toutain, J.-P., 2002. Soil gas profiles as a tool to characterise active tectonic areas: the Jaut Pass example (Pyrenees, France). Earth Planet. Sci. Lett. 196, 69–81.

Brogna, A., La Delfa, S., La Monaca, V., Lo Nigro, S., Morelli, D., Patanè, G., Tringali, G., 2007. Measurements of indoor radon concentration on the south-eastern flank of Mount Etna volcano (southern Italy). J. Volcanol. Geoth. Res. 165, 71–75. doi:10.1016/j.jvolgeores.2007.04.012.

Burton, M., Neri, M., Condarelli, D., 2004. High spatial resolution radon measurements reveal hidden active faults on Mt. Etna. Geophys. Res. Lett. 31 (7), L07618. doi:10.1029/2003GL019181.

Burton, M.R., Neri, M., Andronico, D., Branca, S., Caltabiano, T., Calvari, S., Corsaro, R.A., Del Carlo, P., Lanzafame, G., Lodato, L., Miraglia, L., Salerno, G., Spampinato, L., 2005. Etna 2004–2005: an archetype for geodynamically-controlled effusive eruptions. Geophys. Res. Lett. 32, L09303. doi:10.1029/2005GL022527.

Casillas, R., Nagy, G., Pantó, G., Brändle, J., Fórizs, I., 1995. Occurrence of Th, U, Y, Zr, and REE-bearing accessory minerals in late-Variscan granitic rocks from the Sierra de Guadarrama (Spain). Eur. J. Mineral. 7, 989–1006.

Choubey, V.M., Bist, K.S., Saini, N.K., Ramola, R.C., 1999. Relation between soil-gas radon variation and different lithotectonic units, Garhwal Himalya, India. Appl. Radiat. Isot. 51, 487–592.

Davis, J.C., 1986. Statistics and Data Analysis in Geology. John Wiley and Sons, New York, pp. 646.

Durrani, S.A., 1999. Radon concentration values in the field: correlation with underlying geology. Radiat. Meas. 31, 271–276.

ENSDF, 2011. Evaluated Nuclear Structure Data File. http://www.nndc.bnl.gov/ensdf/index.jsp Retrieved on March 8, 2011.

Giammanco, S., Sims, K.W.W., Neri, M., 2007. Measurements of ^{220}Rn and ^{222}Rn and CO_2 emissions in soil and fumarole gases on Mt. Etna volcano (Italy): implications for gas transport and shallow ground fracture. Geochem. Geophys. Geosyst. 8, Q10001. doi:10.1029/2007GC001644.

Giammanco, S., Bonfanti, P., 2009. Cluster analysis of soil CO_2 data from Mt. Etna (Italy) reveals volcanic influences on temporal and spatial patterns of degassing. Bull. Volcanol. 71, 201–218. doi:10.1007/s00445-008-0218-x.

Giammanco, S., Immè, G., Mangano, G., Morelli, D., Neri, M., 2009. Comparison between different methodologies for detecting radon in soil along an active fault: the case of the Pernicana fault system, Mt. Etna. Appl. Radiat. Isot. 67 (1), 178–185. doi:10.1016/j.apradiso.2008.09.007.

Giammanco, S., Bellotti, F., Groppelli, G., Pinton, A., 2010. Statistical analysis reveals spatial and temporal anomalies of soil CO_2 efflux on Mount Etna volcano (Italy). J. Volcanol. Geotherm. Res. 194, 1–14. doi:10.1016/j.jvolgeores.2010.04.006.

ICRP-65, 1993. Protection against radon-222 at home and at work. Ann. ICRP 23 (2), 45. ICRP Pub. 65.

Immè, G., La Delfa, S., Lo Nigro, S., Morelli, D., Patanè, G., 2006a. Soil radon concentration and volcanic activity of Mt. Etna before and after the 2002 eruption. Radiat. Meas. 41, 241–245.

Immè, G., La Delfa, S., Lo Nigro, S., Morelli, D., Patanè, G., 2006b. Soil radon monitoring in NE flank of Mt. Etna (Sicily). Appl. Radiat. Isot. 64, 624–629.

Imposa, S., Patané, G., 1985. The Fondo Macchia earthquake of october 15, 1911. In: Postpischl, D. (Ed.), Atlas of Isoseismal Maps of Italian Earthquakes. Quad. Ric. Scient., vol. 2A, p. 114. 116–117.

Israel, H., Bjornsson, S., 1967. Radon (Rn-222) and thoron (Rn-220) in soil air over faults. Z. Geophys. 33, 48–64.

Jonsson, G., Baixeras, C., Devantier, R., Enge, W., Font, L.L., Freyer, K., Ghose, R., Treutler, H.-C., 1999. Soil radon levels measured with SSNTD's and the soil radium content. Radiat. Meas. 31, 291–294.

King, C.-H., King, B.-S., Evans, W.C., 1996. Spatial radon anomalies on active faults in California. Appl. Geochem. 11, 497–510.

La Delfa, S., Immè, G., Lo Nigro, S., Morelli, D., Patanè, G., Vizzini, F., 2007a. Radon measurements in the SE and NE flank of Mt. Etna (Italy). Radiat. Meas. 42, 1404–1408.

La Delfa, S., Patanè, G., Presti, F., Tringali, G., 2007b. Changing in crust mechanical behaviour due to raising magma: a fracturing model of SE flank of Mt. Etna (Sicily). Earth Planet. Sci. Lett. 256, 493–509.

Malczewski, D., Żaba, J., 2007. ^{222}Rn and ^{220}Rn concentrations in soil gas of Karkonoszeelzera block (Sudetes, Poland). J. Environ. Radioact. 92, 144–164. doi:10.1016/j.jenvrad.2006.11.001.

Mazur, D., Janik, M., Loskiewicz, J., Olko, P., Swakon, J., 1999. Measurements of radon concentration in soil gas by CR-39 detectors. Radiat. Meas. 31, 295–300.

Monaco, C., De Guidi, G., Catalano, S., Ferlito, C., Tortorici, G., Tortorici, L., 2008. Carta Morfotettonica del Monte Etna. Litografia Artistica Cartografica, Firenze.

Morelli, D., Immè, G., La Delfa, S., Lo Nigro, S., Patanè, G., 2006. Evidence of soil radon as tracer of magma uprising at Mt. Etna. Radiat. Meas. 41, 721–725.

Neri, M., Acocella, V., Behncke, B., 2004. The role of the Pernicana fault system in the spreading of Mt. Etna (Italy) during the 2002–2003 eruption. Bull. Volcanol. 66, 417–430. doi:10.1007/s00445-003-0322-x.

Neri, M., Acocella, V., Behncke, B., Maiolino, V., Ursino, A., Velardita, R., 2005. Contrasting triggering mechanisms of the 2001 and 2002–2003 eruptions of Mount Etna (Italy). J. Volcanol. Geotherm. Res. 144, 235–255. doi:10.1016/j.jvolgeores.2004.11.025.

Neri, M., Behncke, B., Burton, M., Giammanco, S., Pecora, E., Privitera, E., Reitano, D., 2006. Continuous soil radon monitoring during the july 2006 Etna eruption. Geophys. Res. Lett. 33, L24316. doi:10.1029/2006GL028394.

Neri, M., Casu, F., Acocella, V., Solaro, G., Pepe, S., Berardino, P., Sansosti, E., Caltabiano, T., Lundgren, P., Lanari, R., 2009. Deformation and eruptions at Mt. Etna (Italy): a lesson from 15 years of observations. Geophys. Res. Lett. 36, L02309. doi:10.1029/2008GL036151.

Neri, M., Guglielmino, F., Rust, D., 2007. Flank instability on Mount Etna: radon, radar interferometry and geodetic data from the southern boundary of the unstable sector. J. Geophys. Res. 112. doi:10.1029/2006JB004756.

Neri, M., Mazzarini, F., Tarquini, S., Bisson, M., Isola, I., Behncke, B., Pareschi, M.T., 2008. The changing face of Mount Etna's summit area documented with lidar technology. Geophys. Res. Lett. 35, L09305. doi:10.1029/2008GL033740.

Nuclear Wallet Cards, 2009. Nuclear Wallet Cards Database. http://www.nndc.bnl.gov/nudat2/indx_sigma.jsp Retrieved on March 8, 2011.

Sinclair, A.J., 1974. Selection of thresholds in geochemical data using probability graphs. J. Geochem. Explor. 3, 129–149.

Siniscalchi, A., Tripaldi, S., Neri, M., Giammanco, S., Piscitelli, S., Balasco, M., Behncke, B., Magrì, C., Naudet, V., Rizzo, E., 2010. Insights into fluid circulation

across the Pernicana fault (Mt. Etna, Italy) and implications for flank instability. J. Volcanol. Geotherm. Res. 193, 137–142. doi:10.1016/j.jvolgeores.2010.03.013.

Solaro, G., Acocella, V., Pepe, S., Ruch, J., Neri, M., Sansosti, E., 2010. Anatomy of an unstable volcano through in SAR data: multiple processes affecting flank instability at Mt. Etna in 1994–2008. J. Geophys.Res. 115, B10405. doi:10.1029/2009JB000820.

Sonzogni, A., 2008. Interactive Chart of Nuclides. National Nuclear Data Center: Brookhaven National Laboratory. http://www.nndc.bnl.gov/chart/ Retrieved 2008-06-06.

Vaupotič, J., 2003. Indoor radon in Slovenia. Nucl. Technol. Radiat. Prot. 2, 36–43.

Walter, T.R., Acocella, V., Neri, M., Amelung, F., 2005. Feedback processes between magmatism and E-flank movement at Mt. Etna (Italy) during the 2002–2003 eruption. J. Geophys. Res. 110, B10205. doi:10.1029/2005JB003688.

Wang, R.-C., Wang, D.-Z., Zhao, G.-T., Lu, J.-J., Chen, X.-M., Xu, S.-J., 2001. Accessory mineral record of magma–fluid interaction in the Laoshan I- and A-type granitic complex, eastern China. Phys. Chem. Earth PT A: Solid Earth Geodes. 26 (9–10), 835–849. doi:10.1016/S1464-1895(01)00131-4.

WHO-IARC (World Health Organization – International Agency for Research on Cancer) IARC, 1988. Monograph on the Evaluation of Carginogenic Risks to Humans: Man Made Mineral Fibres and Radon, vol. 43. IARC Monograph, Lyon, France.

Žunić, Z.S., Kobal, I., Vaupotič, J., Kozak, K., Mazur, J., Birovljev, A., Janik, M., Čeliković, I., Ujić, P., Demajo, A., Krstić, G., Jakupi, B., Quarto, M., Bochicchio, F., 2006. High natural radiation exposure in radon spa areas: a detailed field investigation in Niška Banja (Balkan region). J. Environ. Radioact. 89, 249–260. doi:10.1016/j.jenvrad.2006.05.010.